The Astrophysical Journal, 635:718–722, 2005 December 10

SURFACE CHARGING AND X-RAY EMISSION FROM INSULATOR SURFACES INDUCED BY COLLISIONS WITH HIGHLY CHARGED IONS: RELEVANCE TO COMETARY AND PLANETARY SPECTROSCOPY

N. Djurić, J. A. Lozano, S. J. Smith, and A. Chutjian
Jet Propulsion Laboratory, California Institute of Technology, Pasadena, CA 91109
Received 2005 April 19; accepted 2005 July 22

ABSTRACT

Characteristic X-ray emission lines are detected from simulants of comet surfaces as they undergo collisions with highly charged ions (HCIs). The HCI projectiles are O^{+2}–O^{+7}. Ion energies are varied in the range $(2–7)q$ keV, where q is the ion charge state. The targets are the insulator minerals olivine, augite, and quartz. It is found that the emission of characteristic K–L, K–M X-rays appears to proceed during positive charging of the surface by the HCI beam. When one uses low-energy, flood-gun electrons to neutralize the surface charge, the X-ray emission is eliminated or greatly reduced, depending on the flood-gun current. Acceleration of background electrons onto the charged surface results in excitation of elemental transitions, including the K–L_2 and K–L_3 target X-ray emission lines of Mg and Si located spectroscopically at 1253.6 and 1739.4 eV, respectively. Also observed are emission lines from O, Na, Ca, Al, and Fe atoms in the target and charge-exchange lines via surface extraction of electrons by the O^{+q} electric field. Good agreement is found in the ratio of the measured X-ray yields for Mg and Si relative to the ratio of their electron-impact K-shell ionization cross sections. The present study may serve as a guide to astronomers as to specific observing X-ray energies indicative of solar/stellar wind or magnetospheric ion interactions with a comet, planetary surface, or circumstellar dust.

Subject headings: atomic processes — comets: general — X-rays: general

1. INTRODUCTION

The spectra of comets, from the infrared to the X-ray regions, have provided a wealth of data on the molecular composition of the comet atmosphere (Dello Russo et al. 2004; Fernández et al. 2003; Mumma et al. 2001) and its interaction with the solar wind (Krasnopolsky et al. 2002; Lisse et al. 2001; Krasnopolsky & Mumma 2001; Greenwood et al. 2001). X-ray production by charge exchange of the cometary gases with highly charged ions (HCIs) in the solar wind has been confirmed in terms of the charge-exchange and X-ray emission channels involved (Greenwood et al. 2004, 2000, 2001; Dalgarno 2003; Kharchenko et al. 2003; Cravens 2002, 2000; Schwadron & Cravens 2000; Beiersdorfer et al. 2003). However, absent in these studies is discussion of the role of a cometary, lunar, or planetary surface. Under what circumstances does the surface contribute, if at all, to X-ray production? At what wavelengths should one observe X-ray emissions resulting from the collision of solar wind HCIs with a comet surface?

To answer these questions, a surface-charging experiment was set up to investigate the interaction of HCIs with mineral targets that are commonly regarded as being simulants of comet surfaces and interstellar material. The minerals chosen were olivine [$(Mg, Fe)_2SiO_4$], augite [(Ca, Na)(Mg, Fe, Al)(Al, $Si)_2O_6$], and quartz (SiO_2). These crystalline silicates have been identified via the Si-O band emissions in circumstellar regions (Justtanont et al. 2004). The production of the mineral X-rays was studied under various conditions of HCI species, charge state, and ion velocity. X-ray emission spectra were measured and shown to be the result of (1) a positive charge buildup on the mineral surfaces caused by ejection of secondary electrons by the HCIs; then (2) acceleration of spurious background electrons back onto the positively charged surface, causing excitation of inner-shell X-ray transitions in the mineral components O, Na, Mg, Al, Si, Ca, and Fe; and (3) charge transfer of the surface electrons with the incident HCI beam to give projectile X-ray $np \rightarrow 1s$ emission lines.

2. EXPERIMENTAL METHODS

The CAPRICE electron-cyclotron resonance ion source at the JPL HCI Facility is used to generate various charge states q of the ions O^{+q} ($q = 2–8$; Chutjian et al. 1999; Greenwood et al. 2000). The ions are extracted from the CAPRICE and accelerated through a potential that was varied in the range 2–7 keV, corresponding to a total ion energy of $(2–7)q$ keV. After mass-to-charge selection, the ions are electrostatically deflected through 45°, transported by an einzel lens system, and focused into the surface-collision (six-way cross) vacuum chamber. Typical ion beam currents (electrical) at the sample target are between 0.1 and 500 nA, with the higher currents obtained at the lower charge states. The vacuum base pressure is approximately 3×10^{-6} Pa.

A schematic diagram of the target holder and the collision region is shown in Figure 1. A titanium holder is mounted to a stainless steel sample arm attached to an off-center rotary motion feedthrough. Clamped to the holder is the target, consisting of a square piece of the mineral of dimensions 5×5 mm^2 and 1–3 mm thick. The HCI beam collides with the target at a 45° angle to the surface normal, and the emitted X-rays are viewed at the specular 45° angle. Depending on the experiment, the stainless steel arm can be either grounded or biased to a specific potential. The holder is rotated out of the HCI beam path to measure the HCI beam current in a downstream Faraday cup. One can also monitor the HCI current on the second position of the target arm using an electrically insulated titanium collector plate (see Fig. 1).

In order to monitor the effects of surface charge, various methods have been used in the literature to change or eliminate surface charges on insulators. The insulator target may be (1) heated to increase its electrical conductivity (e.g., LiF; Auth et al. 1995), (2) prepared as a thin foil over a conducting substrate, (3) covered with a thin conductive film (Carrez et al. 2001) or with a high-transparency mesh, or (4) irradiated with low-energy electrons from a flood gun (Tomizuka & Ayame 1994; Dukes et al. 1999).

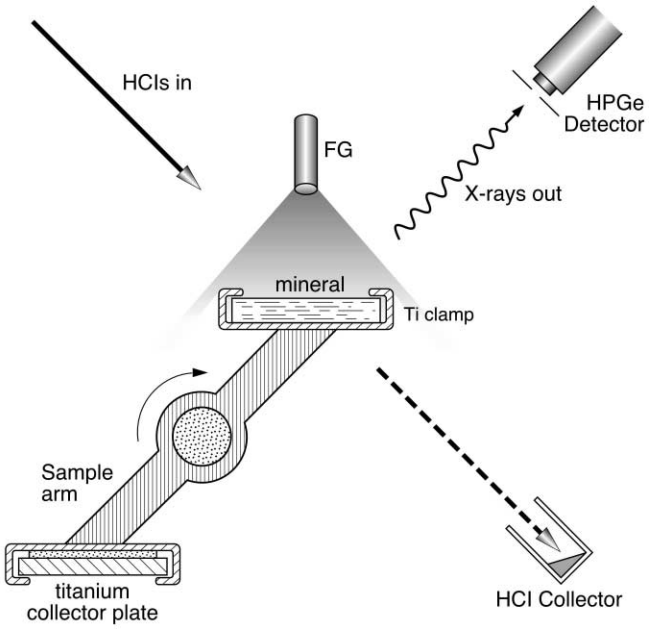

FIG. 1.—Schematic diagram of the collision region containing the isolated conductor or dielectric material. Shown are the incident HCI beam direction and the X-ray viewing direction at 90° to the HCI beam, which define a scattering plane. The flood gun (FG) is located 60° above this plane. Rotation of the sample holder about its axis exposes (here) either the olivine or titanium collector plate to the HCI beam. The incident HCI current is measured with the sample holder rotated into the clear area. The X-ray detector can be either an HPGe detector or a grazing incidence spectrometer with a CCD camera. A simple equivalent circuit of the mounted crystal consists of a leakage resistance R_l and a capacitance C to the sample holder.

The flood gun approach was deemed the simplest and was the method used here.

A commercial gun (used in cathode ray tubes) served as an electron flood gun (FG). It was mounted on the top flange, at an angle of about 75° to the sample normal and above the plane formed by the direction of the HCI beam and X-ray detector axis. The purpose of the FG is to provide a beam of low-energy electrons to neutralize the positive surface charge generated by the HCI beam. The FG energies could be varied in the range 20–100 eV, and currents varied from 2 to 1000 nA. These currents are very likely an underestimate, as they were measured at the smaller, unshielded Ti cover plate.

The X-rays were energy analyzed and detected using a windowed, high-purity Ge (HPGe) solid-state X-ray detector placed at 45° with respect to the surface normal (and 90° with respect to the incident HCI beam direction; see Fig. 1). A 7.5 μm thick Be window isolated the detector from the vacuum chamber. Use of the window introduced a transmission factor depending on the X-ray energy. The X-ray detector was energy calibrated using the 5.89 and 6.49 keV X-rays from a ^{55}Fe isotope. Calibrations were done at two different times: once prior to the start of measurements and once midway through the measurements (six months later). The energy scale for energies below 4 keV was shifted 25 eV to higher energies to correspond more closely to the spectroscopic energies and is accurate to about 20 eV. The resolution was measured to be 105 eV (FWHM) in a separate experiment recording the $np \rightarrow 1s$ emissions in collisions of Ne^{+9} with H_2O and CO_2 gaseous targets.

When a positive ion beam bombards a dielectric or an ungrounded conductor surface, secondary electrons are ejected from a thin surface layer. The surface potential of the dielectric or ungrounded conductor increases until the incident HCI beam current is balanced by incident stray electron currents and outgoing backscattered and secondary electron currents (Hastings & Garrett 1996). The potential at the surface can in principle rise to a maximum value equal to the ion acceleration voltage V_{acc}. In such cases, one can actually stop or reflect the incident ion beam to give rise to a "trampoline effect" at the surface (Burgdörfer et al. 2004).

Stray electron currents are present as a result of the energetic HCI beam hitting lenses, slits, the target holder, the HCI collector, etc. These electrons are available for acceleration into the sample surface. (The effect of photoelectron emission, possibly arising from scattered and reflected X-rays from the target, is a secondary effect and is negligible here.) Measurements were carried out on targets of commercial samples of olivine, augite, and quartz. The olivine was purchased from Gem and Mineral Miners, Inc. (Alta Loma, CA), and the mineral itself was mined from the Datso Mine near Kohestan, Pakistan. The SiO_2 was a commercial quartz microscope slide, and the augite was unpedigreed, commercially available material. For the olivine, a fresh surface was cleaved from a larger stone, and the cleaved fragment was rinsed in ethanol and then mounted and placed in the vacuum chamber. The augite and SiO_2 samples were simply rinsed in trichloroethylene or ethanol before mounting. While there is almost certainly some thin layer of hydrocarbons and other impurities present on all these surfaces, previous experience (Takács et al. 1997) leads one to believe that observations can be made that are of general significance and that the large potential energy stored in the multiply and highly charged ion beams makes X-ray observations from the bulk less sensitive to remaining surface impurities.

3. RESULTS AND DISCUSSION

Results are presented for the projectile ions O^{+q} ($q = 2$–7), and the range of total projectile energy studied is $E = (2.0$–$7.0)q$ keV, or 4.0–49.0 keV. Also measured (not reported here) were X-ray emissions from ions of C, N, Ne, and Ar, in which similar results were observed. The observed X-ray spectra were found to have three components: (1) a broad background (including bremsstrahlung radiation), (2) target X-ray emission peaks of intensity that increased linearly with ion beam current, and (3) projectile X-ray emissions corresponding to the $np \rightarrow 1s$ transitions. The observed broad background radiation was usually indicative of the presence of background electrons. The intensities of all recorded X-ray spectra were affected by the sample alignment with respect to the incoming ions and to the detector position.

Target X-ray emission spectra.—Target X-ray spectra were measured as a function of both ion acceleration voltage and ion charge state. For all spectra the emission intensity was normalized to an X-ray yield Y defined as $Y = (\text{photon counts})(q/I_i)t^{-1}$, where I_i is the ion current (as measured in the HCI collector), I_i/q is the particle current, and t is the time taken to accumulate the spectra (the HCI beam exposure time). Shown in Figure 2 are the yields of the Mg K–$L_{2,3}$, K–$M_{2,3}$; Si K–$L_{2,3}$, K–$M_{2,3}$; and weak O K–L X-rays emitted from an olivine surface for different O^{+q} charge states ($q = 2$–7) at ion energies of 7.0q keV. Also shown are the K–L, M, N, O transitions in O^{+6} lying in the range 570–713 eV. These transitions arise from direct charge exchange of the O^{+7} projectile ions with electrons emitted from the olivine surface. The resolution of the detector (105 eV, FWHM) was insufficient to resolve the fine-structure splitting ($L_{2,3}$, etc.) in these levels. All data have been corrected for transmission of the Be foil detector window. This transmission, as obtained from the manufacturer's supplied data, is less than 0.5% at 400 eV, rising to 20% at 800 eV, 40% at 1000 eV, and 80% at 1800 eV.

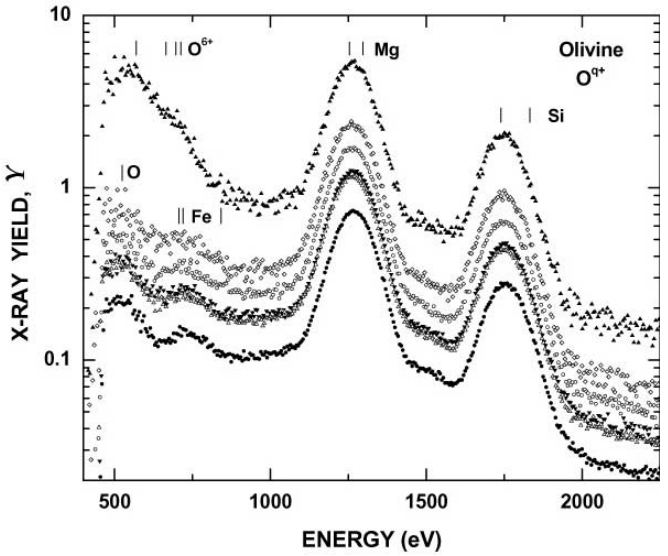

FIG. 2.—Spectral yields *Y* of the O K–L; Mg K–$L_{2,3}$, K–$M_{2,3}$; and Si K–$L_{2,3}$, K–$M_{2,3}$ X-rays emitted from an olivine surface for different O^{+q} charge states and a total ion energy of 7.0*q* keV. (In each case the lower energy line is the unresolved K–$L_{2,3}$ transition.) Also shown is the single feature of unresolved O^{+6} K–L, M, N, O transitions resulting from direct charge exchange of O^{+7} with surface-extracted electrons. The charge states are given by *filled circles,* $q = 2$; *open triangles,* $q = 3$; *filled inverted triangles,* $q = 4$; *open circles,* $q = 5$; *diamonds,* $q = 6$; and *filled triangles,* $q = 7$. All spectra here and in Figs. 3–5 have been corrected for transmission of the Be window of the HPGe detector.

Shown in Figure 3 are spectral yields of the O K–L; Mg K–L, M; Si K–L, M; and Fe L–M X-rays emitted from the interaction of O^{+3} with an olivine surface. Measurements were taken at six O^{+3} energies in the range 2.7–7.0 keV.

Examples of X-ray spectra during irradiation of augite and quartz targets are shown in Figures 4 and 5, respectively. The augite spectrum is particularly rich and consists of the peaks near 1253.6 and 1739.4 eV arising from the K–L, M transitions in Mg and Si, respectively. Also detected are X-rays of O, Na, Mg, Al, Fe, and Ca associated with the other mineral components.

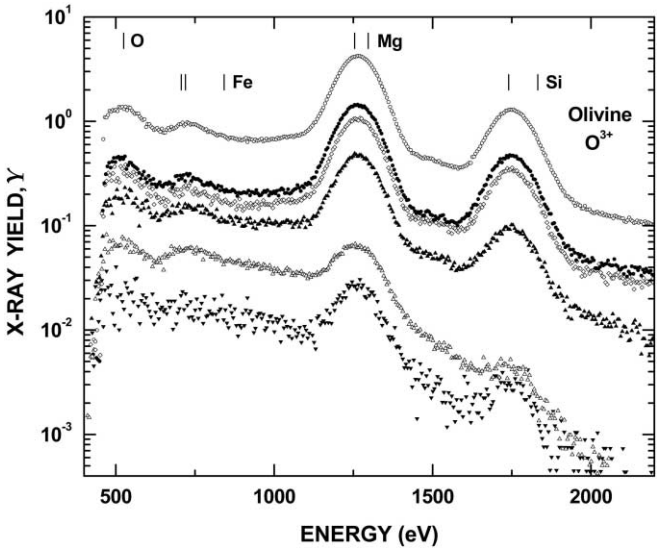

FIG. 3.—Spectral yields *Y* of the K–$L_{2,3}$ and K–$M_{2,3}$ target X-ray lines emitted from an olivine surface for O, Mg, and Si X-rays. The projectile is O^{+3}, and the energy notation is *filled inverted triangles,* 2.7 keV; *open triangles,* 3.0 keV; *filled triangles,* 4.0 keV; *diamonds,* 5 keV; *filled circles,* 6.0 keV; and *open circles,* 7.0 keV.

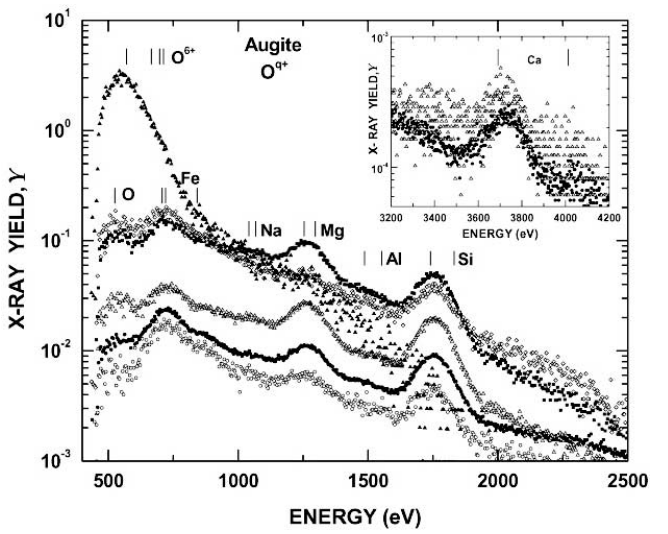

FIG. 4.—X-rays emitted from a sample of augite bombarded by O^{+q} ions at energies of 7.0*q* keV. The charge states are given by *filled circles,* $q = 2$; *open triangles,* $q = 3$; *open circles,* $q = 4$; *squares,* $q = 5$; *diamonds,* $q = 6$; and *filled triangles,* $q = 7$. Spectral yields *Y* of the K–$L_{2,3}$ and K–$M_{2,3}$ transitions are indicated for Na, O, Mg, Al, Si, and Ca (as the inset) and for the L–M transition in Fe. Also shown is the single feature of unresolved O^{+6} K–L, M, N, O transitions resulting from direct charge exchange of O^{+7} with surface-extracted electrons.

The spectrum of SiO_2 in Figure 5 is less complex. It consists of only the Si and O transitions. Two features are worthy of note here: (1) The Si K–L, M and O K–L emissions are absent with the FG turned on, i.e., when V_{surf} is reduced below that required to generate a K-shell hole in the Si and O atomic components of SiO_2. This result is again evidence that the role of the HCI beam is to produce a surface potential V_{surf} to accelerate ambient electrons and ionize K- or L-shell electrons in the mineral components. (2) The unresolved K–L, M, N, O emissions in O^{+6} remain strong with the FG on. This feature arises from charge exchange, with electrons "pulled" from the mineral surface by the electric field of the O^{+7} beam (see below).

Time constant of the X-ray emission.—One would like to obtain an estimate of the time constant of the surface charging

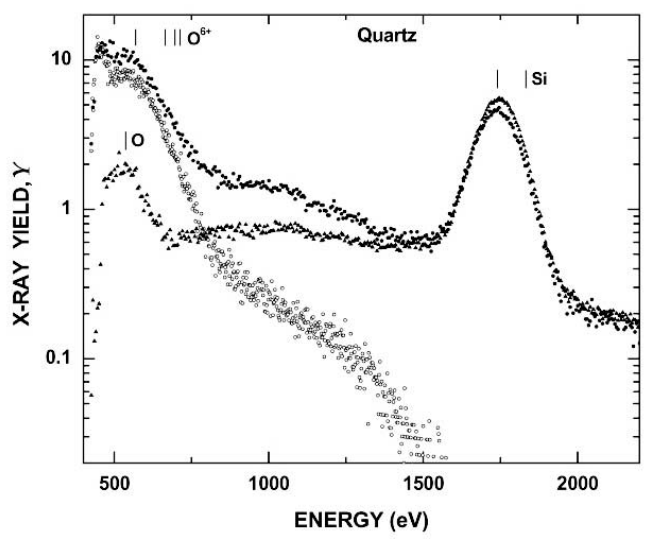

FIG. 5.—Spectral yields *Y* of the K–$L_{2,3}$ and K–$M_{2,3}$ X-rays emitted by O and Si from a quartz (SiO_2) surface for the projectile O^{+3} or O^{+7} ion, together with the single feature of unresolved O^{+6} K–L, M, N, O transitions resulting from direct charge exchange of O^{+7} with surface-extracted electrons. The notation is *filled circles,* O^{+7}; *open circles,* O^{+7} with the FG turned on; and *triangles,* O^{+3}.

and neutralization process. Experiments were carried out with a phase- and amplitude-modulated FG (electron beam) and a phase-modulated ion beam. The ion beam could be modulated to a rate greater than 1 MHz, and the FG could be modulated only up to 1 kHz due to limitations of electron focusing. The relative timing between the electron and ion signals could be set to better than 0.1 ms. The X-ray emission was monitored during the different phase modulation conditions. The FG electrons sharply affected the emission by neutralization of the surface charge and effectively eliminated the X-ray emission in a time of less than 10 ms after turn-on. The relation (seen empirically to be linear) between surface charge density σ and the surface potential $V_{\rm surf}(P)$ (at a point P a distance r from the mineral) is simply given as $V_{\rm surf}(P) = (4\pi\varepsilon_0)^{-1} \int_a (\sigma/r)\, da$. (Here ε_0 is the permittivity of free space and da is a surface area element of the mineral.) The surface charging was also reversible: when the FG was turned off, with the ion beam on, the X-ray emission returned to its original intensity (to within the 10 ms window).

An equivalent circuit of the mineral target is a leakage resistance R_l in parallel with a capacitance C of the mineral. As an order-of-magnitude approximation, one may calculate the time constant $\tau = R_l C$ of this circuit as approximately a leakage resistance of 10^8–10^9 Ω times the mineral capacitance of 10 pF, or $\tau = 1$–10 ms. This is in approximate agreement with experiment.

Finally, the X-ray emission was found to increase linearly with ion current. This observation is consistent with the fact that increasing ion fluxes lead to a higher flux of background electrons to the surface and hence a higher excitation rate of X-rays—provided that $eV_{\rm surf}$ exceeds the target K- and L-shell electron-impact ionization potentials.

Projectile emission spectra.—One sees in Figures 2–5 the unresolved K–L, M, N, O X-ray emissions from O^{+6} that arise from direct charge exchange of the O^{+7} projectile with electrons. In particular, from Figure 5 one sees that this feature persists when the FG is turned on, whereas the Si K–L, M mineral lines are absent. This is evidence for two separate mechanisms at work—X-rays from the target and X-rays from the projectile—and the result is again consistent with the observation that surface X-rays are caused only when one has a positively charged surface (FG off). This effect involving the FG is perhaps the clearest method of distinguishing between these two sources of emission, where ambiguity may exist.

The projectile charge-exchange X-rays arise from electrons that are "pulled" toward the HCI beam by the large HCI-surface electric field. To estimate the effect of this electric field, for a charge state of $q = 7$ the first electron can be emitted from the surface starting at a distance of about 20 au (Bardsley & Penetrante 1991). The bound electrons in both the insulating and conducting targets are able to respond to the fast approach of the ion to the target. The timescale of the surface response is given by the inverse of the plasmon frequency, or about 10^{-16} s, whereas the time it takes an inclined beam (45°) of 50 keV O^{+7} ions to enter and leave a region 100 au from the surface is of the order 10^{-14} s, or about 100 times slower than the solid's response (Apell 1987).

Target X-rays are only observed when the mineral surface remains positively charged, i.e., when the FG is turned off. With the FG turned on, $V_{\rm surf}$ and the subsequent X-ray emissions are reduced or eliminated. The reduction of the X-ray emission was found to be linear with increasing FG electron current (as measured on the Ti collector plate). It appears that the roles of the ion beam are both to charge the surface and to contribute a background of eligible electrons. The X-rays are thus created in the following sequence: (1) the surface is positively charged by the ion beam impact; (2) background electrons are created by the ion beam at slits, at lenses, from the target itself, etc.; (3) these electrons are accelerated onto the target and remove core K-shell electrons from the mineral's atomic components; and (4) the core vacancies fill via transitions from higher levels that give rise to the characteristic X-rays. The target X-rays are not produced when (5) the FG is turned on, lowering $V_{\rm surf}$.

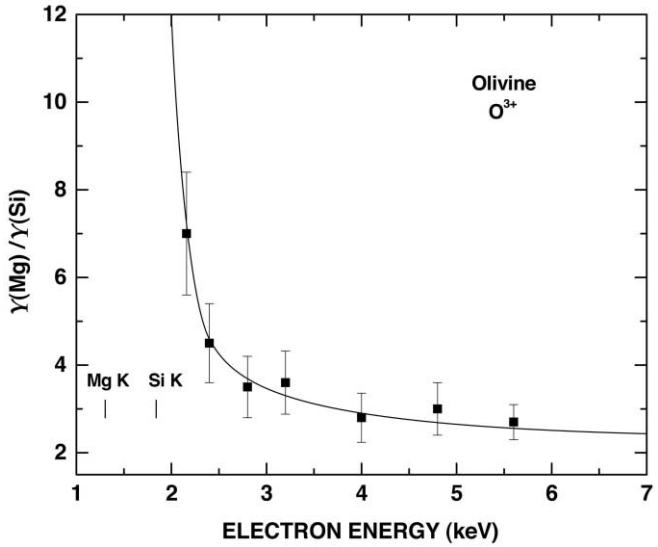

FIG. 6.—Measured ratio of the Mg and Si X-ray yields Y(Mg)/Y(Si) (*squares*) as a function of a scaled surface energy given as $eV_{\rm surf} = 0.8eV_{\rm acc}$. Shown for comparison is the calculated ratio of K-shell ionization cross sections for Mg and Si (*solid line*; Santos et al. 2003). The ionization thresholds for Mg and Si are indicated by the vertical bars.

One diagnostic for this scenario is that a threshold effect should be observable: no X-rays can be emitted if the energy of the electron incident on the surface is less than the K-shell binding energy of the electron in the target atom. Since the charging potential induced at the sample surface can be as high as the ion acceleration voltage $eV_{\rm acc}$, the total background electron current (the sum of backscattered, secondary, and stray currents) may strike the surface with energies as high as $eV_{\rm acc}$. Shown in Figure 6 are the ratios Y(Mg)/Y(Si) of the experimental X-ray emission yields for Mg and Si in an olivine target, as obtained from spectra such as those shown in Figure 3. The ratio is plotted as a function of a scaled surface energy $eV_{\rm surf}$. All yields were corrected for the underlying bremsstrahlung background, as well as the Be window transmission.

Cross sections for electron-impact ionization of K-shell electrons have been calculated for Mg and Si atoms by Santos et al. (2003) using a binary-encounter Bethe model. These results are also included in Figure 6. In scaling the electron energy axis, one can assume a potential $V_{\rm surf} < V_{\rm acc}$ to account for partial charge neutralization by the impact of background electrons or from electron leakage currents. Here, good agreement with the shape of the Santos et al. cross section ratios was obtained by scaling the experimental electron energy axis as $eV_{\rm surf} = 0.8eV_{\rm acc}$. The comparisons in Figure 6 show relatively constant ratios at energies between 7 and 3 keV. From the Wannier Law, the cross section for ionization approaches zero at the threshold. This is evident in Figure 6 in that the ratios rise steeply as one approaches, at first, the zero cross section at the Si K-shell threshold energy. The good agreement between the ratio of yields and that of ionization cross sections lends support to the model in which the X-rays are created by ionization of Mg and Si K-shell electrons by surface-accelerated background electrons.

The target K-shell radiation is caused by electron-impact ionization of the K-shell electrons in the mineral components. Previous experiments on collisions of Ar^{+17} with SiO_2 also observed target X-rays and projectile radiation (Takács et al. 2001; Lehnert et al. 1998). The appearance of silicon K-shell X-ray radiation was explained in Takács et al. by photoionization of the target atoms by the energetic (4.12 keV) Ar K-shell X-rays. The same explanation cannot be applied here, since the projectile O^{+6} $K–L_{2,3}$ transition energies (<700 eV) are significantly lower than the binding energy of the Mg (1.30 keV) and Si (1.84 keV) K-shell electrons (Fig. 6).

Finally, it is interesting to note recent cases in which mineral X-rays have been detected in a planetary object. Trombka et al. (2000) have observed K-shell X-rays of Mg, Si, and Fe at asteroid 433 Eros, and Wargelin et al. (2004) have detected O, Mg, Al, and Si K-shell X-rays from the sunlit lunar side. In both cases the mechanism was concluded to be fluorescence caused by the solar X-ray spectrum. However, Elsner et al. (2002) detected X-ray emission in the energy range 300–1890 eV from Io and Europa (and possibly Ganymede). At these distances, the solar X-ray flux is a negligible contributor to the X-ray emission intensity. Rather, they conclude that the X-rays are powered by the energetic H^+, O^+, and S^+ ion population in the Io plasma torus (IPT). One could speculate that the satellite surfaces become charged by the energetic ion bombardment, and the charged surfaces accelerate the low-energy (<700 eV) IPT electrons to create K-shell holes. On the other hand, there is a good supply of energetic (MeV) electrons in the Jovian magnetosphere, and hence surface charging/acceleration would not be required for hole production. Possibly, both mechanisms are at work.

4. CONCLUSIONS

The results of this study indicate that characteristic emission lines from O, Na, Mg, Al, Si, Ca, Fe, and possibly other mineral components should be observable when a solar or stellar wind, or a magnetospheric ion, impinges on dust, a circumstellar object, or a satellite having a composition resembling that of olivine, forsterite, or orthopyroxene. The following are also required for the emission to occur: (1) The surface must become charged by the solar/stellar wind impact; hence, the surface must be electrically nonconducting. (2) The surface potential V_{surf} must exceed the ionization potential of the K- and L-shell electrons. (3) Background electrons must be present. Requirement 2 is fulfilled by having an ion impact energy greater than about 1.30 keV for Mg and 1.84 keV for Si. Such energies are available in the solar wind. For example, the abundant O^{+6} ion can have a distribution of energies around 46.7 and 13.3 keV in the fast (750 km s^{-1}) and slow (400 km s^{-1}) solar wind, respectively (Schwadron & Cravens 2000). The background electrons in requirement 3 can arise from solar or stellar UV and X-ray photoionization of the cometary surface and/or by secondary electrons produced by the solar or stellar wind impact.

We thank J.-K. Kim for providing us with calculated electron-impact cross sections for K-shell ionization of Si. N. Dj. and J. A. L. thank the National Research Council for support under the NASA-NRC Fellowship program. This work was carried out at the Jet Propulsion Laboratory, California Institute of Technology, and was supported by the National Aeronautics and Space Administration through agreement with Caltech.

REFERENCES

Apell, P. 1987, Nucl. Instrum. Methods Phys. Res. B, 23, 242
Auth, C., Hecht, T., Igel, T., & Winter, H. 1995, Phys. Rev. Lett., 74, 5244
Bardsley, J. N., & Penetrante, B. M. 1991, Comments At. Mol. Phys., 27, 43
Beiersdorfer, P., et al. 2003, Science, 300, 1558
Burgdörfer, J., Wirtz, L., Reinhold, C. O., & Lemell, C. 2004, Vacuum, 73, 3
Carrez, P., Leroux, H., Cordier, P., & Guyot, F. 2001, Philos. Mag. A, 81, 2823
Chutjian, A., Greenwood, J. B., & Smith, S. J. 1999, in AIP Conf. Proc. 475, Application of Accelerators in Research and Industry, ed. J. L. Duggan & I. L. Morgan (New York: AIP), 881
Cravens, T. E. 2000, Adv. Space Res., 26, 1443
———. 2002, Science, 296, 1042
Dalgarno, A. 2003, Ap&SS, 285, 687
Dello Russo, N., Disanti, M. A., Magee-Sauer, K., Gibb, E. L., Mumma, M. J., Barber, R. J., & Tennyson, J. 2004, Icarus, 168, 186
Dukes, C. A., Baragiola, R. A., & McFadden, L. A. 1999, J. Geophys. Res., 104, 1865
Elsner, R. F., et al. 2002, ApJ, 572, 1077
Fernández, Y. R., Meech, K. J., Lisse, C. M., A'Hearn, M. F., Pittichová, J., & Belton, M. J. S. 2003, Icarus, 164, 481
Greenwood, J. B., Mawhorter, R. J., Cadez, I., Lozano, J., Smith, S. J., & Chutjian, A. 2004, Phys. Scr., T110, 358
Greenwood, J. B., Williams, I. D., Smith, S. J., & Chutjian, A. 2000, ApJ, 529, 605
———. 2001, Phys. Rev. A, 63, 062707
Hastings, D., & Garrett, H. 1996, Spacecraft-Environment Interactions (Cambridge: Cambridge Univ. Press), chap. 5
Justtanont, K., de Jong, T., Tielens, A. G. G. M., Feuchtgruber, H., & Waters, L. B. F. M. 2004, A&A, 417, 625
Kharchenko, V., Rigazio, M., Dalgarno, A., & Krasnopolsky, V. A. 2003, ApJ, 585, L73
Krasnopolsky, V. A., Christian, D. J., Kharchenko, V., Dalgarno, A., Wolk, S. J., Lisse, C. M., & Stern, S. A. 2002, Icarus, 160, 437
Krasnopolsky, V. A., & Mumma, M. J. 2001, ApJ, 549, 629
Lehnert, U., Stockli, M. P., & Cocke, C. L. 1998, J. Phys. B, 31, 5117
Lisse, C. M., Christian, D. J., Dennerl, K., Meech, K. J., Petre, R., Weaver, H. A., & Wolk, S. J. 2001, Science, 292, 1343
Mumma, M. J., et al. 2001, ApJ, 546, 1183
Santos, J. P., Parente, F., & Kim, Y.-K. 2003, J. Phys. B, 36, 4211
Schwadron, N. A., & Cravens, T. E. 2000, ApJ, 544, 558
Takács, E., Berényi, Z., Gillaspy, J. D., Ratliff, L. P., Minniti, R., Pedulla, J., Deslattes, R. D., & Stolterfoht, N. 2001, J. Phys. B, 34, 1277
Takács, E., Ónodi-Szücs, Z. Ratliff, L. P., Gillaspy, J. D., & Pálinkás, J. 1997, Nucl. Instrum. Methods B, 124, 431
Tomizuka, H., & Ayame, A. 1994, Anal. Sci., 10, 633
Trombka, J. I., et al. 2000, Science, 289, 2101
Wargelin, B. J., Markevitch, M., Juda, M., Kharchenko, V., Edgar, R., & Dalgarno, A. 2004, ApJ, 607, 596